

# Single-Molecule Characterization of van der Waals Contact Between Alkane and Gold

Hongyu Ju<sup>1,2†</sup>, Jinying Wang<sup>2,3†</sup>, Wangping Liu<sup>4†</sup>, Jie Hao<sup>2†</sup>, Mengmeng Li<sup>2</sup>, Yanxia Xu<sup>2</sup>, Boyu Wang<sup>2</sup>, Suhang He<sup>2</sup>, Kunrong Mei<sup>1\*</sup>, Andrew C.-H. Sue<sup>5\*</sup>, Keqiu Chen<sup>4\*</sup>, Chuancheng Jia<sup>2\*</sup> & Xuefeng Guo<sup>2,6\*</sup>

<sup>1</sup>School of Pharmaceutical Science and Technology, Tianjin University, Tianjin 300072, <sup>2</sup>Center of Single-Molecule Sciences, Institute of Modern Optics, Frontiers Science Center for New Organic Matter, Tianjin Key Laboratory of Microscale Optical Information Science and Technology, College of Electronic Information and Optical Engineering, Nankai University, Tianjin 300350, <sup>3</sup>Network for Computational Nanotechnology, Purdue University, West Lafayette, Indiana 47907, <sup>4</sup>Department of Applied Physics, School of Physics and Electronics, Hunan University, Changsha 410082, <sup>5</sup>College of Chemistry and Chemical Engineering, Xiamen University, Xiamen 361005, <sup>6</sup>Beijing National Laboratory for Molecular Sciences, National Biomedical Imaging Center, College of Chemistry and Molecular Engineering, Peking University, Beijing 100871

\*Corresponding authors: [guoxf@pku.edu.cn](mailto:guoxf@pku.edu.cn); [jiacc@nankai.edu.cn](mailto:jiacc@nankai.edu.cn); [keqiuchen@hnu.edu.cn](mailto:keqiuchen@hnu.edu.cn); [andrewsue@xmu.edu.cn](mailto:andrewsue@xmu.edu.cn); [kmei@tju.edu.cn](mailto:kmei@tju.edu.cn); †H. Ju, J. Wang, W. Liu, and J. Hao contributed equally to this work.

Cite this: CCS Chem. 2024, Just Published. DOI: 10.31635/ccschem.024.202403861

Van der Waals (vdW) contact, dominated by weak but ubiquitous vdW interactions, plays a significant role in diverse fields such as supramolecular chemistry, nanotechnology, and surface science. Accurate characterization of vdW contact at the single-molecule level remains challenging. Herein, we combine the scanning tunneling microscope break junction technique with first-principles calculations to study the mechanical and electrical characteristics of the alkane/Au vdW contact in an in-situ solution environment. The step-like conductance plateaus indicate a gradual desorption of alkyl chains in units of two methylene groups under force stretching. Two distinct charge transport channels, through the shortest C-H/Au pathway and the entire adsorbed alkyl chain, are identified. Furthermore, we discover that a higher electric field leads to increased conductance and stronger bonding of the alkane/Au vdW contact. These results unveil the intrinsic properties of vdW contact at the molecular and even atomic levels,

which are crucial for exploring noncovalent interactions and advancing molecular sciences.



**Keywords:** alkane, van der Waals contact, single-molecule electronics, scanning tunneling microscope break junction, electric field

## Introduction

The organic/metal interface is scientifically and technologically important in a wide variety of applications including catalysis, surface science, and organic electronics.<sup>1–4</sup> In particular, van der Waals (vdW) contact between organic molecules and metals, characterized by weak yet ubiquitous interactions.<sup>5,6</sup> However, the interfacial properties of vdW contact remain poorly understood.<sup>7</sup> On one hand, interfaces between massive molecules and metals possess various structural and chemical disorders that may generate uncontrolled influences and fundamentally alter the interfacial properties.<sup>5</sup> On the other hand, accurate identification and measurement of vdW interactions, which are the weakest interactions at the atomic level, from interacting systems is highly challenging.<sup>8,9</sup> The situation at the solid-liquid interface becomes more complicated due to the interference from solvent molecules.<sup>10</sup> Hence, accurate characterization of the molecule/metal vdW contact at the single-molecule level has long been desired to explore and apply their intrinsic properties efficiently.<sup>11–13</sup>

Alkane/Au contact, which represents one of the most important types of vdW contact, shows relatively simple vdW interactions and has been extensively studied in surface science.<sup>14–16</sup> Alkanes have long served as a model molecule for investigating vdW interactions and exploring processes such as sorption/desorption and surface self-assembly.<sup>17–20</sup> In addition, alkyl groups are commonly used to modulate interfacial coupling and electronic structures in molecular devices.<sup>21,22</sup> The scanning tunneling microscope break junction (STM-BJ) technique has emerged as a powerful tool for characterizing noncovalent interactions and interfacial contact in solution at the single-molecule level from an electrical perspective. It allows the detection of  $\sigma$ - $\sigma$  stacking interactions and the conversion between chemisorption and physisorption.<sup>23–26</sup> A more profound exploration of the mechanisms and potential applications of the alkane/Au vdW contact can be anticipated through the careful selection of characteristic molecules and the application of a directional electric field in STM-BJ.<sup>27,28</sup>

Herein, we investigate the structural evolution and corresponding charge transport mechanism of alkane/Au vdW contact through STM-BJ experiments and first-principles calculations. Our results demonstrate that alkyl chains are peeled off from the gold surface in units of two methylene groups under force stretching, corresponding to the step-like conductance plateaus observed in 1-octanethiol. Two distinct charge transport channels are identified: one along the entire alkyl chain and the other along the shortest C–H/Au pathway. Significantly, both conductance and bonding strength of alkane/Au vdW contact exhibit distinct bias dependence, with a higher

bias voltage leading to increased conductance and stronger bonding.

## Experimental Methods

### Conductance measurement

The gold tip (99.99%) is controlled by a stepper motor and a piezo stack to repeatedly bring into and out of contact with the gold substrate (99.99%). Before each experiment, the gold substrate is annealed with a butane flame for ~30 s. The current between the tip and substrate is measured continuously in 1,2,4-trichlorobenzene (TCB) solution containing 1 mM target molecule, unless otherwise mentioned. The conductance versus displacement traces during the STM tip retraction are used in all analyses. The stretching rate of the tip is about 9.3 nm s<sup>−1</sup>. Single-molecule conductance measurements are carried out by an X-TECH STM-BJ technique, and the data are analyzed by the XMe open-source code ([https://github.com/Pilab-XMU/XMe\\_DataAnalysis](https://github.com/Pilab-XMU/XMe_DataAnalysis)).<sup>29</sup>

### Flicker noise analysis

During STM tip retraction, if the sampling points around the most likely conductance value exceed a certain threshold, it means that a conductance plateau has emerged. Then, the movement of the tip is stopped at the position where the molecular junction is formed and held for 150 ms with a sampling rate of 20 kHz per second. A square of the discrete Fourier transform of a conductance curve is calculated to obtain the noise power spectral density. More than 10,000 conductance traces are recorded to get the two-dimensional (2D) histogram of the flicker noise power spectra.

### I–V characterization

When a molecular junction is formed, the tip is paused and the measurement mode is changed to carry out I–V measurements with a bias range of ±1 V, which finishes in a duration of 150 ms in our experiments. After the I–V measurement, the mode is automatically switched to current-time curve measurements. If the measured conductance still falls within the preset conductance range, the measured I–V curve is collected for the statistical analysis. The 2D I–V, as well as 2D G–V histograms are plotted in a 150 × 150 array.

### Computational methods

The geometry optimization and transmission coefficient  $T(E)$  of the single-molecule device are carried out by using the generalized gradient approximation Perdew–Burke–Ernzerhof exchange-correlation functional with the non-equilibrium Green's function approach in the QuantumATK package.<sup>30,31</sup> The electrode is built to be large enough to eliminate the effect of other molecules in

the periodic direction. Fritz-Haber-Institute pseudopotential is used for calculating both geometry optimization and transmission curves with the single-Zeta polarized basis set for Au atoms and the double-Zeta polarized for other atoms. In order to consider vdW forces between the molecule and electrodes, density functional theory calculations with dispersion corrections of Grimme (Grimme-DFT-D2) are taken into account as a correction of energy.<sup>32</sup> In specifics, the optimization is converging with the 0.02 eV/Å force tolerance, the energy cutoff is 150 Ry, iteration control tolerance is  $1 \times 10^{-5}$ ,  $k$ -point sampling is Monkhorst-Pack type.  $k$ -point sampling perpendicular to the electron transport is  $k_A = k_B = 2$ ,  $k_C = 150$  in the parallel transport direction when calculating the transmission curve. The conductance  $\sigma(\mu)$  is calculated using the Landauer formula.

## Results and Discussion

### Desorption of alkyl chains from the Au surface

To investigate the vdW interactions between alkane and gold, the charge transport properties of dynamic

single-molecule junctions that are composed of 1-alkanethiol and asymmetric contacts (one robust Au-S covalent contact and the other C-H/Au vdW contact) are measured via a STM-BJ technology (Figure 1a). Specifically, the single-molecule conductance is measured repeatedly with tip-substrate displacements. The process involves creating and disrupting single-molecule junctions in a solution of TCB containing the target molecule at a concentration of 1 mM. Typical individual traces for 1-octanethiol under 0.2 V bias are presented as a purple line in Figure 1b and Supporting Information Figure S1. The conductance features four-step continuous conductance plateaus. These findings suggest that the four conductance states (I, II, III, and IV) are part of a continuous and correlated process. A 2D conductance-displacement histogram consisting of thousands of such conductance-displacement traces is plotted in Figure 1b and further confirms the four conductance states. A plausible hypothesis explaining the four conductance states is that mono-thiol-anchored alkane can form stable alkane/Au vdW contact with varying geometries when connected to the gold substrate. The one-dimensional (1D) conductance

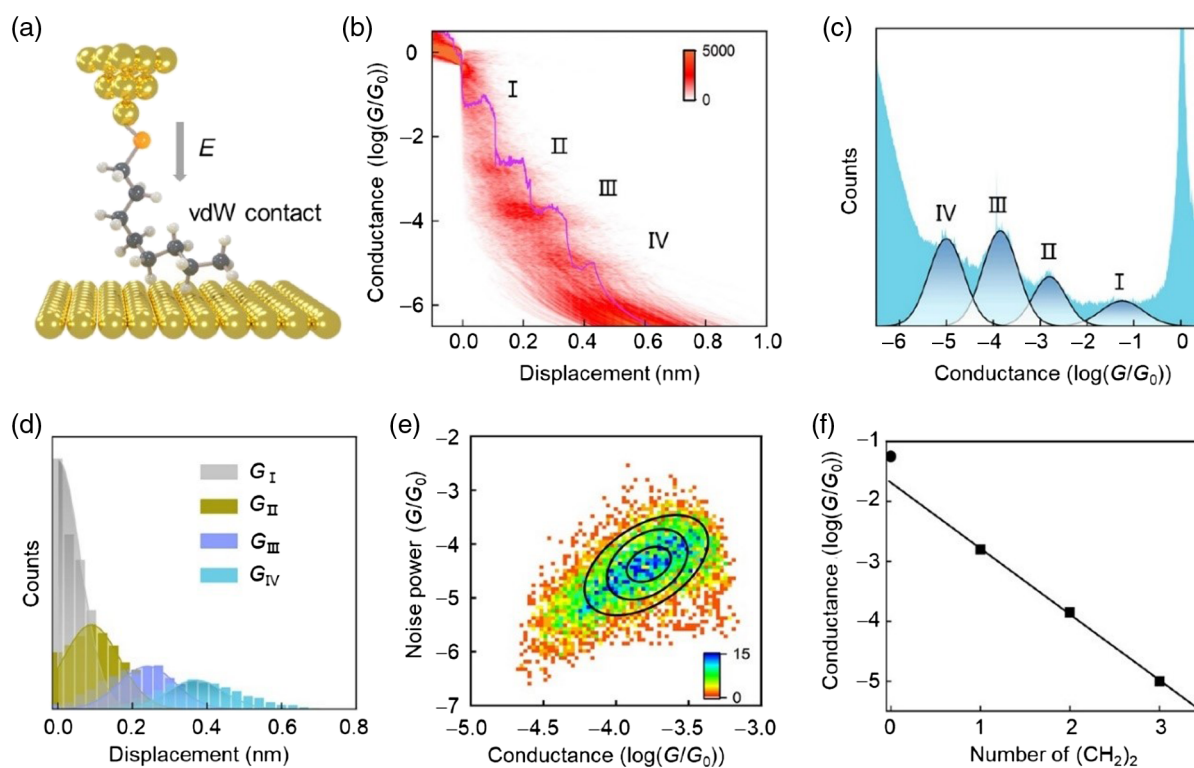


**Figure 1 |** Break junction measurements of 1-octanethiol. (a) Schematic STM-BJ measurements of the vdW contact between alkane and gold.  $E$  represents the bias-induced oriented electrical field. (b) 2D conductance-displacement histogram of 1-octanethiol. One typical single conductance-displacement trace with four distinct plateaus is marked. (c) 1D logarithmic conductance histogram of 1-octanethiol. (d) Junction displacement distributions of molecular junctions corresponding to the four conductance states in panel (b). (e) 2D histogram of normalized flicker noise power versus average conductance for 1-octanethiol junctions corresponding to state III. (f) The conductance at the peak for four states versus the number of suspended methylene groups.

histogram provides a statistical analysis of the conductance peaks (Figure 1c), whose maximum frequencies are located at  $10^{-1.25} G_0$ ,  $10^{-2.80} G_0$ ,  $10^{-3.85} G_0$ , and  $10^{-5.00} G_0$  (where  $G_0 = 2e^2/h = 77.5 \mu\text{S}$  is the quantum conductance) from state I to state IV, respectively. The formation of vdW contact is further supported by control experiments (Supporting Information Figure S2), where the conductance states cannot be observed in 0.01 mM TCB solutions. The displacement length of the junctions is analyzed to gain deeper insights into the evolution of the junction structure during stretching. As shown in Figure 1d, the junction displacement gradually increases from conductance state I to state IV. The increment of displacement between adjacent states, from state II to state IV, is about 0.15 nm, implying a continuous and repetitive process during the stretching. Note that the displacement of state I is considerably small due to the snapback distance of the Au atoms after breakdown. Furthermore, the measurement using a preassembled monolayer sample shows that the observed four conductance states are independent on the adsorption site of the monothiol group (Supporting Information Figure S3).

The charge transport through molecule/metal contact is strongly dependent on interfacial coupling, involving both through-bond and through-space couplings, which can be assessed by the flicker noise analysis. Flicker noise analyses conducted on 1-octanethiol show the noise power scales to be  $G^{1.97}$  across the conductance states, indicating the charge transport through junctions is dominated by through-space coupling (Figure 1e and Supporting Information Figure S4).<sup>25,33</sup> This is because weak through-space coupling induces more interfacial fluctuations, while robust through-bond coupling restrains the fluctuations. Consequently, these results further support the finding that the four conductance states arise from distinct alkane/Au vdW contact.

In the nonresonant tunneling regime of molecular junctions, conductance typically decays as  $G \sim e^{-\beta N}$ , where  $\beta$  is the decay constant and  $N$  is the unit number of the molecular backbone. The  $\beta$  values of alkane have been extensively measured using difunctionalized molecules with different lengths, ranging from 0.91 to 1.02 in previous studies.<sup>34–37</sup> In our continuous measurements, a linear fit of conductance values for states II to IV yields a  $\beta$  value of 1.05 (Figure 1f). This continuous measurement approach gives a  $\beta$  value similar to those obtained in previous discrete and independent measurements, indicating a desorption process of alkane on the metal surface. Extrapolating the fit to zero units reveals a contact resistance of  $\sim 600 \text{ k}\Omega$  ( $0.021 G_0$ ) for the molecular junction, meeting the minimum value ( $1/G_0$ ) dictated by fundamental quantum mechanics for a single conducting channel across a junction.<sup>36,37</sup> Surprisingly, this asymmetric junction, including vdW contact, exhibits a relatively low contact resistance, comparable in magnitude to SMe ( $270 \text{ k}\Omega$ )

and  $\text{NH}_2$  ( $370 \text{ k}\Omega$ ) anchors.<sup>38,39</sup> For the conductance state I, the measured conductance value is slightly higher than  $0.021 G_0$  due to efficient charge transport pathways offered by both alkane/Au and S/Au contacts in the narrow gap.

To understand the desorption process of alkane on the metal surface, the bond angle between the molecular anchoring group and the Au tip, as well as the zigzag carbon skeleton in alkyl chains should be considered. For alkanethiol adsorbed on a gold surface, the Au-S-C bond angle is about  $104^\circ$ , and the backbone tilts at about  $35^\circ$  with respect to the surface under the restriction of molecular bond angles.<sup>40,41</sup> Considering the conductance decay constant and the zigzag carbon skeleton in 1-octanethiol, it is speculated that every two methylene groups are peeled off from the gold substrate simultaneously, leading to the four conductance states for 1-octanethiol. In comparison, we also conduct STM-BJ measurements of 1-hexanethiol and find three conductance states (Supporting Information Figure S5). Besides, previous experimental and theoretical studies have shown that alkane generally adopts a zigzag lying conformation (the methylene groups alternate between high and low positions above the surface) rather than a standing conformation on the metal surface.<sup>42</sup> Two-methylene group desorption offers novel insights into the force-induced desorption of alkane on the gold surface. In the force-induced desorption process of alkane on metal, the adjacent displacement increment obeys  $\Delta Z = (Z_0 + kF)$ , where  $Z_0$  is the length of two methylene,  $k$  is the spring constant of alkane, and  $F$  is the rupture force in break junctions. Our measured increment is less than theoretical  $\Delta Z$ , indicating that the strength of alkane/Au vdW contact is quite weak in solution.

### Charge transport mechanism of alkane/Au vdW contact

First-principles simulation of the desorption process of alkane on the gold surface is conducted to prove our speculation. Four stable configurations of alkane/Au contact are identified by increasing the gap size (Figure 2a). Consistent with previous studies,<sup>14,43</sup> the bonding energy linearly increases with the number of adsorbed methylene groups, measuring approximately  $-2.61$ ,  $-2.03$ ,  $-1.24$ , and  $-0.51 \text{ eV}$ , respectively. The transmission spectra for the four configurations show their conductance near the Fermi level align well with the experimentally observed four conductance states, indicating that the conductance states I, II, III, and IV correspond to the configurations with  $N_{\text{ads}} = 8, 6, 4$ , and  $2$ , respectively (Figure 2b). Notably, all four configurations show a prominent transmission peak around  $-0.32 \text{ eV}$ , corresponding to the alkane/Au coupling. As the Au tip displaces from the substrate, a small transmission peak emerges around  $-0.08 \text{ eV}$  for configurations with  $N_{\text{ads}}$  of  $8$  and  $6$ , and it is masked by the large

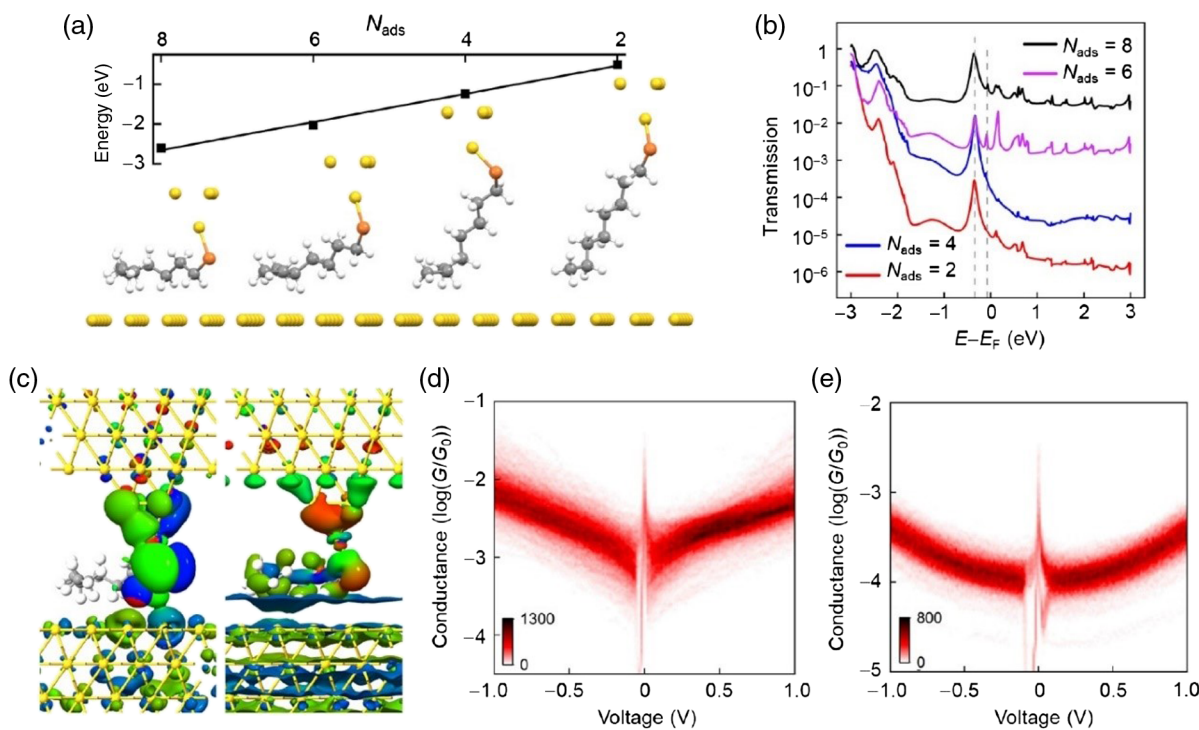


**Figure 2 | Charge transport mechanism of vdW contact.** (a) Optimized configurations (bottom) of 1-octanethiol for four conductance states and the corresponding bonding energies (top), respectively. (b) Transmission curves for four conductance states. (c) Transmission eigenstates for conductance state I at  $-0.32$  eV (left) and  $-0.08$  eV (right). 2D G-V histogram of 1-octanethiol for conductance states II (d) and III (e).

transmission peak at  $-0.32$  eV for the other two configurations. Further analysis of the transmission eigenstates near  $-0.32$  and  $-0.08$  eV indicates the presence of two distinct charge transport channels in all alkane/Au vdW contact: one along the shortest C-H/Au anchoring pathway ( $-0.32$  eV) and the other along the entire adsorbed alkyl chain ( $-0.08$  eV) to pass between electrodes (see the transmission eigenstates of state I or  $N_{ads} = 8$  in Figure 2c and those of state II or  $N_{ads} = 6$  in Supporting Information Figure S6). These results are consistent with the analysis of molecular projected self-consistent Hamiltonian eigenstates (Supporting Information Figure S7).<sup>44</sup> It is worth noting that due to a certain degree of overlap between the two transmission peaks, two transport channels contribute to the measured conductance at the same time. Meanwhile, when two transport channels enter the bias window, the shortest C-H/Au anchoring pathway ( $-0.32$  eV) contributes more to the conductance. To gain further insights into the single-molecule vdW contact, we measure the current versus voltage ( $I$ - $V$ ) and conductance versus voltage ( $G$ - $V$ ) characteristics of 1-octanethiol-based junctions. By bridging a molecule between two electrodes, the current is recorded when scanning the bias voltage between  $\pm 1$  V. The collected  $I$ - $V$  traces are used to construct 2D  $I$ - $V$  histograms. A significant feature is that the conductance of four states of 1-octanethiol increases by

approximately an order of magnitude as the bias changes from 0 to  $\pm 1$  V (Figure 2d,e, and Supporting Information Figure S8), despite having a large highest occupied molecular orbital (HOMO)-lowest unoccupied molecular orbital (LUMO) gap ( $-6.32$  and  $0.82$  eV for HOMO and LUMO, respectively, Supporting Information Figure S9). Furthermore, the conductance changes nearly linearly with the increase in bias for states I and II, while the conductance for state III varies little within a small bias ranging from  $-0.5$  to  $0.5$  V.

To distinguish vdW contact from covalent contact, we conduct both experimental and computational investigations on a single-molecule junction featuring symmetric covalent Au-S contacts established through 1,8-octanedithiol (Figure 3a). In alignment with previous studies,<sup>1,45</sup> a distinct conductance state at  $10^{-4.40}$   $G_0$  is identified, corresponding to the dual Au-S anchored configuration (Figure 3b,c). Meanwhile, the conductance states resulting from a vdW contact are also observed occasionally in the measurements (Supporting Information Figure S10). The noise power scale of  $G^{1.10}$  further demonstrates that the charge transport through 1,8-octanedithiol is dominated by through-bond coupling (inset in Figure 3c and Supporting Information Figure S11), rather than through-space coupling observed in the 1-octanethiol junctions. The results reflect the coupling difference between covalent contact and vdW contact. Similar to 1-octanethiol,

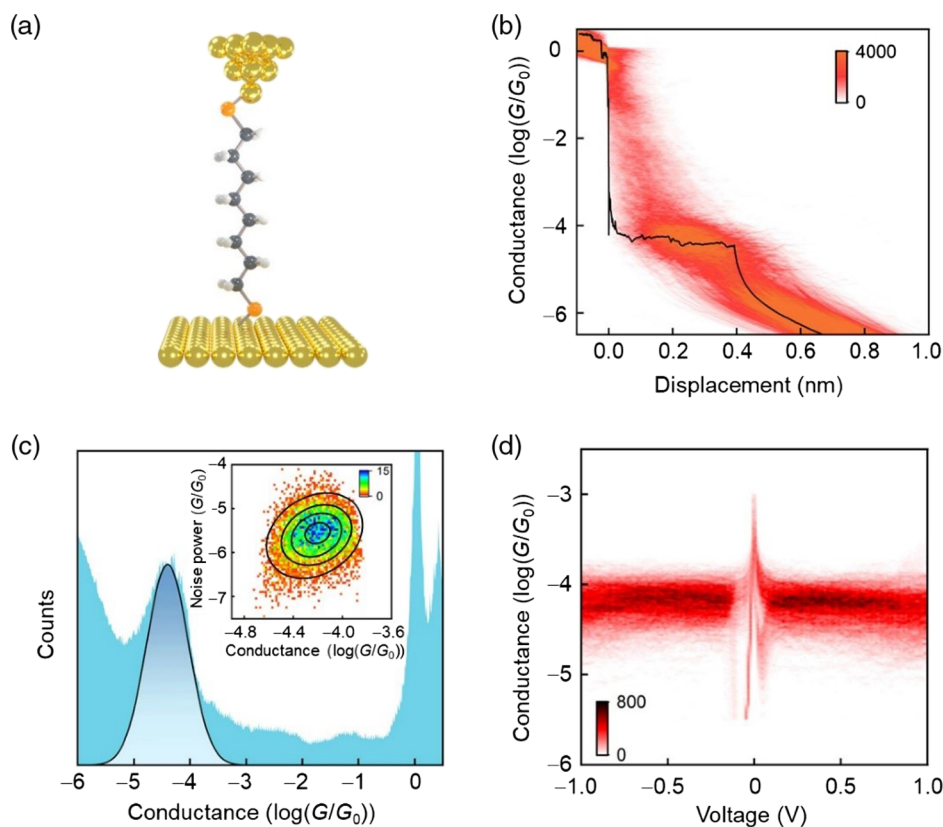


**Figure 3 | Break junction measurements of 1,8-octanedithiol.** (a) Schematic STM-BJ measurements of double covalent-anchored contacts. (b) 2D conductance-displacement histogram of 1,8-octanedithiol. The typical single conductance trace is marked. (c) 1D logarithmic conductance histogram of 1,8-octanedithiol. The inset shows the 2D histogram of normalized flicker noise power versus average conductance. (d) 2D G-V histogram of 1,8-octanedithiol.

1,8-octanedithiol exhibits a large HOMO-LUMO gap ( $-6.37$  and  $0.77$  eV for HOMO and LUMO, respectively, [Supporting Information Figure S12](#)). Its transmission spectrum displays a prominent peak at  $-1.18$  eV, but the transmission peak at  $-0.32$  eV vanishes ([Supporting Information Figure S13](#)), corresponding to the absence of vdW contact. Furthermore,  $I$ - $V$  measurements indicate that the conductance of 1,8-octanedithiol remains nearly constant across the studied bias range, aligning with previous research (Figure 3d and [Supporting Information Figure S14](#)).<sup>34,46</sup> The disparate bias responses in the 1,8-octanedithiol and 1-octanethiol systems highlight the finding that vdW contact exhibits a more conspicuous bias response in comparison with covalent contact.

### Bias dependence of alkane/Au vdW contact

Although alkane is generally regarded as a nonpolar molecule, it exhibits high polarizability, reaching up to  $\sim 15.9$  Å<sup>3</sup> in previous studies.<sup>47</sup> This high polarizability renders alkanes highly responsive to external electric fields.<sup>48</sup> Numerous studies have demonstrated that the bias electric field in STM-BJ can regulate the molecular reaction dynamics and configurations.<sup>27,49</sup> Therefore, we

propose an electric field-dependent vdW contact model (Figure 4a). If a nonpolar entity is subjected to an applied electric field, it triggers a rearrangement of charge distribution, resulting in the formation of an induced dipole moment ( $P_{\text{induced}}$ ). Considering the accumulation of electrons at the electrode, both electrostatic and inductive forces are amplified, fortifying the vdW contact. The differential charge density is used to visualize the electron characteristics of vdW contact under a bias electric field. In comparison with the case under a zero-electric field, an obvious enhancement in the differential charge density is observed at the alkane/Au interface under an electric field of  $0.5$  eV/Å (Figure 4b). Moreover, we confirm the bias response of the vdW contact through bias-dependent stretching break junction measurements (Figure 4c-f, and [Supporting Information Figure S15](#)). The conductance plateaus become more pronounced under a higher bias voltage, indicating the higher formation probability and bonding strength of the vdW contact. According to the nature of alkane, increased induction and dispersion forces are mainly responsible for higher bonding strength. The polarization-induced enhancement of vdW contact is expected to be a fundamental phenomenon under bias. This bias-dependent

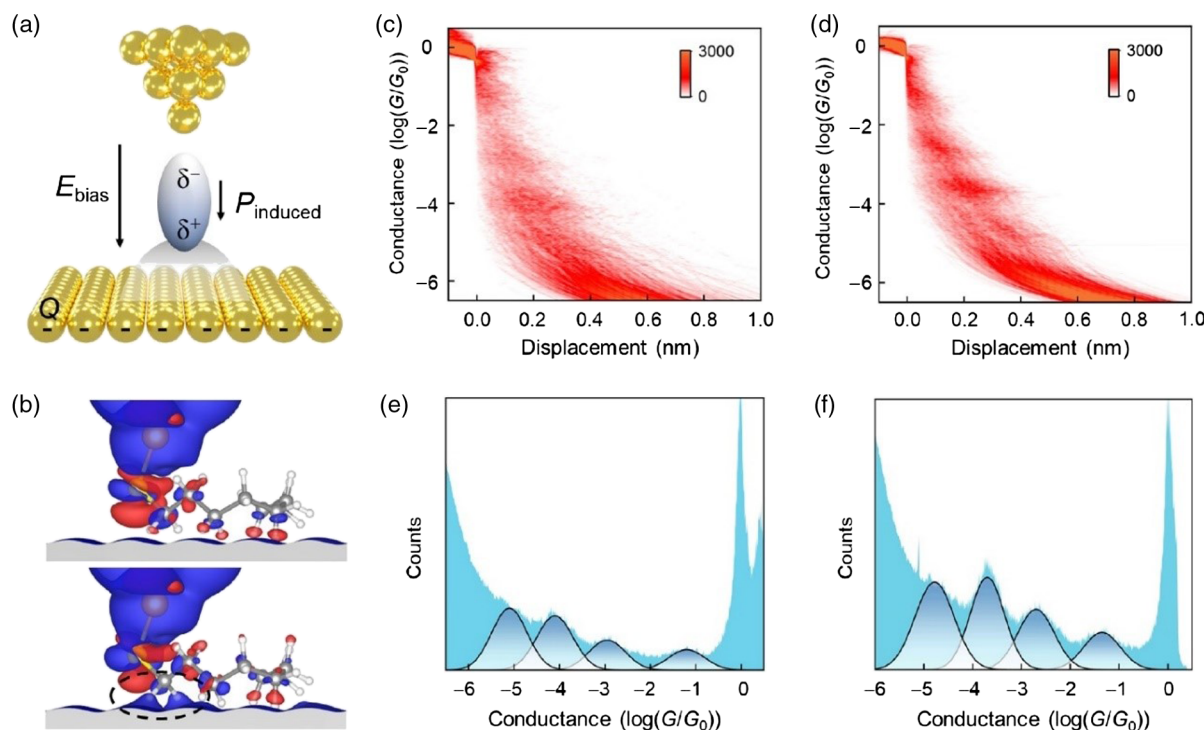


**Figure 4 | Bias-dependent break junction measurements of 1-octanethiol.** (a) A model of bias electric field-induced strengthening for vdW contact. (b) Differential charge densities without electric field (top) and under electric field 0.5 eV/Å (bottom) (blue: positive; red: negative). The isosurface level is 0.0012. 2D conductance-displacement histogram of 1-octanethiol at bias 0.1 V (c) and 0.4 V (d). 1D logarithmic conductance histogram of 1-octanethiol at bias 0.1 V (e) and 0.4 V (f).

effect can potentially be used to fabricate molecular devices or investigate the electrical field effect at the single-molecule level by regarding the entity polarizability as a microprobe.

## Conclusion

In this study, we combine the STM-BJ technique and first-principles calculations to characterize the desorption process of alkane from the gold surface and explore the charge transport mechanism of alkane/Au vdW contact at the single-molecule level in an in-situ solution environment at room temperature. Our results reveal that alkyl chains are peeled off from the gold surface in units of two methylene groups, resulting in four distinct vdW contacts and their corresponding conductance states for 1-octanethiol junctions. Two distinct charge transport channels are identified, one along the shortest C-H/Au atomic contact and the other along the entire alkyl chain. In addition, both the conductance and the bonding strength of the alkane/Au vdW contact exhibit clear bias dependence. These findings not only provide a strategic framework for exploring noncovalent interactions, but also offer novel insights into molecular device fabrication and field-effect investigations.

## Supporting Information

Supporting Information is available and includes conductance measurements, flick noise analyses,  $I-V$  measurements, and theoretical data.

## Conflict of Interest

There is no conflict of interest to report.

## Funding Information

We acknowledge primary financial support from the National Key R&D Program of China (grant nos. 2021YFA1200102, 2021YFA1200101, and 2022YFE0128700), the National Natural Science Foundation of China (grant nos. 22173050, 22150013, 21727806, 21933001, and 11974106), the New Cornerstone Science Foundation through the XPLOSER PRIZE, the Natural Science Foundation of Beijing (grant no. 2222009), Beijing National Laboratory for Molecular Sciences (grant no. BNLMS202105), the Fundamental Research Funds for the Central Universities (grant no. 63223056), and the Frontiers Science Center for New

Organic Matter at Nankai University (grant no. 63181206).

## References

- Inkpen, M. S.; Liu, Z. F.; Li, H.; Campos, L. M.; Neaton, J. B.; Venkataraman, L. Non-Chemisorbed Gold-Sulfur Binding Prevails in Self-Assembled Monolayers. *Nat. Chem.* **2019**, *11*, 351–358.
- Chen, H.; Zhang, W.; Li, M.; He, G.; Guo, X. Interface Engineering in Organic Field-Effect Transistors: Principles, Applications, and Perspectives. *Chem. Rev.* **2020**, *120*, 2879–2949.
- Dief, E. M.; Low, P. J.; Díez-Pérez, I.; Darwish, N. Advances in Single-Molecule Junctions as Tools for Chemical and Biochemical Analysis. *Nat. Chem.* **2023**, *15*, 600–614.
- Fahlman, M.; Fabiano, S.; Gueskine, V.; Simon, D.; Berggren, M.; Crispin, X. Interfaces in Organic Electronics. *Nat. Rev. Mater.* **2019**, *4*, 627–650.
- Li, W.; Gong, X.; Yu, Z.; Ma, L.; Sun, W.; Gao, S.; Koroglu, C.; Wang, W.; Liu, L.; Li, T.; Ning, H.; Fan, D.; Xu, Y.; Tu, X.; Xu, T.; Sun, L.; Wang, W.; Lu, J.; Ni, Z.; Li, J.; Duan, X.; Wang, P.; Nie, Y.; Qiu, H.; Shi, Y.; Pop, E.; Wang, J.; Wang, X. Approaching the Quantum Limit in Two-Dimensional Semiconductor Contact. *Nature* **2023**, *613*, 274–279.
- Qian, Q.; Ren, H.; Zhou, J.; Wan, Z.; Zhou, J.; Yan, X.; Cai, J.; Wang, P.; Li, B.; Sofer, Z.; Li, B.; Duan, X.; Pan, X.; Huang, Y.; Duan, X. Chiral Molecular Intercalation Superlattices. *Nature* **2022**, *606*, 902–908.
- Liu, Y.; Weiss, N. O.; Duan, X.; Cheng, H.-C.; Huang, Y.; Duan, X. van der Waals Heterostructures and Devices. *Nat. Rev. Mater.* **2016**, *1*, 1–17.
- Yang, L.; Adam, C.; Nichol, G. S.; Cockroft, S. L. How Much Do van der Waals Dispersion Forces Contribute to Molecular Recognition in Solution? *Nat. Chem.* **2013**, *5*, 1006–1010.
- He, S.; Biedermann, F.; Vankova, N.; Zhechkov, L.; Heine, T.; Hoffman, R. E.; De Simone, A.; Duignan, T. T.; Nau, W. M. Cavitation Energies Can Outperform Dispersion Interactions. *Nat. Chem.* **2018**, *10*, 1252–1257.
- Cai, W.; Xu, D.; Qian, L.; Wei, J.; Xiao, C.; Qian, L.; Lu, Z. Y.; Cui, S. Force-Induced Transition of  $\pi$ - $\pi$  Stacking in A Single Polystyrene Chain. *J. Am. Chem. Soc.* **2019**, *141*, 9500–9503.
- Aradhya, S. V.; Frei, M.; Hybertsen, M. S.; Venkataraman, L. van der Waals Interactions at Metal/Organic Interfaces at the Single-Molecule Level. *Nat. Mater.* **2012**, *11*, 872–876.
- Cai, W.; Xiao, C.; Qian, L.; Cui, S. Detecting van der Waals Forces Between a Single Polymer Repeating Unit and a Solid Surface in High Vacuum. *Nano Res.* **2018**, *12*, 57–61.
- Wang, P.; Jia, C.; Huang, Y.; Duan, X. van der Waals Heterostructures by Design: From 1D and 2D to 3D. *Matter* **2021**, *4*, 552–581.
- Wetterer, S. M.; Lavrich, D. J.; Cummings, T.; Bernasek, S. L.; Scoles, G. Energetics and Kinetics of the Physisorption of Hydrocarbons on Au(111). *J. Phys. Chem. B* **1998**, *102*, 9266–9275.
- Marchenko, A.; Lukyanets, S.; Cousty, J. Adsorption of Alkanes on Au(111): Possible Origin of STM Contrast at the Liquid/Solid Interface. *Phys. Rev. B* **2002**, *65*, 045415.
- Mete, E.; Yortanli, M.; Danisman, M. F. A van der Waals DFT Study of Chain Length Dependence of Alkanethiol Adsorption on Au(111): Physisorption vs. Chemisorption. *Phys. Chem. Chem. Phys.* **2017**, *19*, 13756–13766.
- Xia, T. K.; Landman, U. Molecular Dynamics of Adsorption and Segregation from An Alkane Mixture. *Science* **1993**, *261*, 1310–1312.
- Badia, A.; Lennox, R. B.; Reven, L. A Dynamic View of Self-Assembled Monolayers. *Acc. Chem. Res.* **2000**, *33*, 475–481.
- Tsuzuki, S.; Honda, K.; Uchimaru, T.; Mikami, M. Magnitude of Interaction Between N-Alkane Chains and Its Anisotropy: High-Level Ab Initio Calculations of n-Butane, n-Petane, and n-Hexane Dimers. *J. Phys. Chem. A* **2004**, *108*, 10311–10316.
- Zhong, D. Y.; Franke, J. H.; Podiyannachari, S. K.; Blomker, T.; Zhang, H. M.; Kehr, G.; Erker, G.; Fuchs, H.; Chi, L. Linear Alkane Polymerization on a Gold Surface. *Science* **2011**, *334*, 213–216.
- Swaminathan, N.; Henning, A.; Jurca, T.; Hayon, J.; Shalev, G.; Rosenwaks, Y. Effect of Varying Chain Length of N-Alcohols and N-Alkanes Detected with Electrostatically-Formed Nanowire Sensor. *Sens. Actuators B Chem.* **2017**, *248*, 240–246.
- Han, Y.; Nickle, C.; Zhang, Z.; Astier, H.; Duffin, T. J.; Qi, D.; Wang, Z.; Del Barco, E.; Thompson, D.; Nijhuis, C. A. Electric-Field-Driven Dual-Functional Molecular Switches in Tunnel Junctions. *Nat. Mater.* **2020**, *19*, 843–848.
- Garner, M. H.; Li, H.; Chen, Y.; Su, T. A.; Shangguan, Z.; Paley, D. W.; Liu, T.; Ng, F.; Li, H.; Xiao, S.; Nuckolls, C.; Venkataraman, L.; Solomon, G. C. Comprehensive Suppression of Single-Molecule Conductance Using Destructive  $\sigma$ -Interference. *Nature* **2018**, *558*, 415–419.
- Tang, Y.; Zhou, Y.; Zhou, D.; Chen, Y.; Xiao, Z.; Shi, J.; Liu, J.; Hong, W. Electric Field-Induced Assembly in Single-Stacking Terphenyl Junctions. *J. Am. Chem. Soc.* **2020**, *142*, 19101–19109.
- Feng, A.; Zhou, Y.; Al-Shebami, M. A. Y.; Chen, L.; Pan, Z.; Xu, W.; Zhao, S.; Zeng, B.; Xiao, Z.; Yang, Y.; Hong, W.  $\sigma$ - $\sigma$  Stacked Supramolecular Junctions. *Nat. Chem.* **2022**, *14*, 1158–1164.
- Li, P.; Chen, Y.; Wang, B.; Li, M.; Xiang, D.; Jia, C.; Guo, X. Single-Molecule Optoelectronic Devices: Physical Mechanism and Beyond. *Opto-Electron. Adv.* **2022**, *5*, 210094.
- Aragones, A. C.; Haworth, N. L.; Darwish, N.; Ciampi, S.; Bloomfield, N. J.; Wallace, G. G.; Diez-Perez, I.; Coote, M. L. Electrostatic Catalysis of a Diels-Alder Reaction. *Nature* **2016**, *531*, 88–91.
- Yang, C.; Liu, Z.; Li, Y.; Zhou, S.; Lu, C.; Guo, Y.; Ramirez, M.; Zhang, Q.; Li, Y.; Liu, Z.; Houk, K.; Zhang, D.; Guo, X.

- Electric Field-Catalyzed Single-Molecule Diels-Alder Reaction Dynamics. *Sci. Adv.* **2021**, *7*, eabf0689.
29. Pan, Z.; Dong, G.; Shang, C.; Li, R.; Gao, T.; Lin, L.; Duan, H.; Li, X.; Bai, J.; Lai, Y.; Wu, W.; Shi, J.; Liu, J.; Hong, W. Xme - Xiamen Molecular Electronics Code: An Intelligent and Open-Source Data Analysis Tool for Single-Molecule Conductance Measurements. *Chin. J. Chem.* **2024**, *42*, 317–329.
30. Taylor, J.; Guo, H.; Wang, J. Ab Initio Modeling of Quantum Transport Properties of Molecular Electronic Devices. *Phys. Rev. B* **2001**, *63*, 245407.
31. Brandbyge, M.; Mozos, J. L.; Ordejon, P.; Taylor, J.; Stokbro, K. Density-Functional Method for Nonequilibrium Electron Transport. *Phys. Rev. B* **2002**, *65*, 165401.
32. Grimme, S. Semiempirical GGA-Type Density Functional Constructed with a Long-Range Dispersion Correction. *J. Comput. Chem.* **2006**, *27*, 1787–1799.
33. Li, X.; Zheng, Y.; Zhou, Y.; Zhu, Z.; Wu, J.; Ge, W.; Zhang, Y.; Ye, Y.; Chen, L.; Shi, J.; Liu, J.; Bai, J.; Liu, Z.; Hong, W. Supramolecular Transistors with Quantum Interference Effect. *J. Am. Chem. Soc.* **2023**, *145*, 21679–21686.
34. Li, X. L.; He, J.; Hihath, J.; Xu, B. Q.; Lindsay, S. M.; Tao, N. J. Conductance of Single Alkanedithiols: Conduction Mechanism and Effect of Molecule-Electrode Contact. *J. Am. Chem. Soc.* **2006**, *128*, 2135–2141.
35. Venkataraman, L.; Klare, J. E.; Tam, I. W.; Nuckolls, C.; Hybertsen, M. S.; Steigerwald, M. L. Single-Molecule Circuits with Well-Defined Molecular Conductance. *Nano Lett.* **2006**, *6*, 458–462.
36. Park, Y. S.; Whalley, A. C.; Kamenetska, M.; Steigerwald, M. L.; Hybertsen, M. S.; Nuckolls, C.; Venkataraman, L. Contact Chemistry and Single-Molecule Conductance: A Comparison of Phosphines, Methyl Sulfides, and Amines. *J. Am. Chem. Soc.* **2007**, *129*, 15768–15769.
37. Cheng, Z. L.; Skouta, R.; Vazquez, H.; Widawsky, J. R.; Schneebeli, S.; Chen, W.; Hybertsen, M. S.; Breslow, R.; Venkataraman, L. In Situ Formation of Highly Conducting Covalent Au-C Contact for Single-Molecule Junctions. *Nat. Nanotechnol.* **2011**, *6*, 353–357.
38. Moreno-Garcia, P.; Gulcur, M.; Manrique, D. Z.; Pope, T.; Hong, W.; Kaliginedi, V.; Huang, C.; Batsanov, A. S.; Bryce, M. R.; Lambert, C.; Wandlowski, T. Single-Molecule Conductance of Functionalized Oligoynes: Length Dependence and Junction Evolution. *J. Am. Chem. Soc.* **2013**, *135*, 12228–12240.
39. Zang, Y.; Pinkard, A.; Liu, Z.; Neaton, J. B.; Steigerwald, M. L.; Roy, X.; Venkataraman, L. Electronically Transparent Au-N Bonds for Molecular Junctions. *J. Am. Chem. Soc.* **2017**, *139*, 14845–14848.
40. de la Llave, E.; Clarenc, R.; Schiffrin, D. J.; Williams, F. J. Organization of Alkane Amines on a Gold Surface: Structure, Surface Dipole, and Electron Transfer. *J. Phys. Chem. C* **2013**, *118*, 468–475.
41. Du, W.; Han, Y.; Hu, H.; Chu, H.; Annadata, H. V.; Wang, T.; Tomczak, N.; Nijhuis, C. A. Directional Excitation of Surface Plasmon Polaritons via Molecular Through-Bond Tunneling Across Double-Barrier Tunnel Junctions. *Nano Lett.* **2019**, *19*, 4634–4640.
42. Li, X.; Niu, K.; Zhang, J.; Yu, X.; Zhang, H.; Wang, Y.; Guo, Q.; Wang, P.; Li, F.; Hao, Z.; Xu, C.; Tang, Y.; Xu, Z.; Lu, S.; Liu, P.; Xue, G.; Wei, Y.; Chi, L. Direct Transformation of N-Alkane into All-Trans Conjugated Polyene via Cascade Dehydrogenation. *Nat. Sci. Rev.* **2021**, *8*, nwab093.
43. Baxter, R. J.; Teobaldi, G.; Zerbetto, F. Modeling the Adsorption of Alkanes on an Au(111) Surface. *Langmuir* **2003**, *19*, 7335–7340.
44. Zhang, L.; Li, H.; Feng, Y. P.; Shen, L. Diverse Transport Behaviors in Cyclo[18]Carbon-Based Molecular Devices. *J. Phys. Chem. Lett.* **2020**, *11*, 2611–2617.
45. Xu, B.; Xiao, X.; Tao, N. J. Measurements of Single-Molecule Electromechanical Properties. *J. Am. Chem. Soc.* **2003**, *125*, 16164–16165.
46. Guo, S.; Hihath, J.; Díez-Pérez, I.; Tao, N. Measurement and Statistical Analysis of Single-Molecule Current–Voltage Characteristics, Transition Voltage Spectroscopy, and Tunneling Barrier Height. *J. Am. Chem. Soc.* **2011**, *133*, 19189–19197.
47. Applequist, J.; Carl, J. R.; Fung, K.-K. Atom Dipole Interaction Model for Molecular Polarizability. Application to Polyatomic Molecules and Determination of Atom Polarizabilities. *J. Am. Chem. Soc.* **1972**, *94*, 2952–2960.
48. Chen, X.; Hou, L.; Li, W.; Li, S. Influence of Electric Field on the Viscosity of Waxy Crude Oil and Micro Property of Paraffin: A Molecular Dynamics Simulation Study. *J. Mol. Liq.* **2018**, *272*, 973–981.
49. Wei, Y.; Li, L.; Greenwald, J. E.; Venkataraman, L. Voltage-Modulated van der Waals Interaction in Single-Molecule Junctions. *Nano Lett.* **2023**, *23*, 567–572.